Original article

Ahmed A. Hamza, Taha Z. N. Sokkar*, Mohammed A. El-Bakary and Amira A. S. Azzam

A quantitative study on using digital photoelasticity for characterising the effect of the stretching speed on the necking phenomenon

https://doi.org/10.1515/polyeng-2020-0163
Received July 2, 2020; accepted August 4, 2020; published online August 28, 2020

Abstract: The digital photoelastic technique is used to characterise the necking behaviour of isotactic polypropylene (iPP) fibres. The effect of stretching rate on necking initiation is studied. The birth of necking is observed using photoelastic patterns of the stretched fibres to understand how the localised difference between the principle stresses grows to form a necking region. Finally, the formation of multiple necking regions is characterised photoelastically. These multiple necks are initiated using the same formation mechanism and conditions as if there is only a single necking region. It was evident that, fast stretching causes faster arrangement of molecular chains and hence decreases the time required for necking initiation. Recommendations are suggested for optimum mechanical processing conditions of iPP fibres to avoid failure by necking. Photoelastic patterns are given for illustration.

Keywords: birefringence; necking; photoelasticity; polariscope; polypropylene; stress analysis.

1 Introduction

The mechanical response of polymers, especially polymeric fibres, strongly relies upon temperature, stress and processing time. Controlling these parameters yields a better polymeric structure. Digital stress analysis is finding the *in situ* stress values at different points along the fibre by comparing the captured photoelastic pattern to precomputed photoelastic orders, i.e. lookup tables. This analysis is a well-known technique for characterising polymeric fibres during the mechanical processing of these fibres [1]. It is important to find the distribution of the intrinsic stresses inside the fibre. It can be helpful to understand different mechanical mechanisms such as necking and crazing. Load cells and strain gauges are practical tools for rapid calculation of the stress-strain behaviour [2]. Although these sensing elements provide stress measurements at high accuracy, different regions along the fibre cannot be characterised during dynamic tests. For example, at the necking regions, the intrinsic stresses, i.e. the internal temporary state of stress corresponding to the applied load leading to a temporary *in situ* birefringence (anisotropy) at this region, have different values for the undrawn and drawn zones along the fibre. The available stress sensors cannot distinguish between the undrawn intrinsic stresses, which is the stress values determined at the undrawn regions of the fibre, and the values at the drawn regions. Accordingly, a full-field stress measurement of the distribution of the stress values at the points of the fibre captured in a single image frame, which is limited by the observable field of the polariscope, is recommended for such measurements [3]. Most stress measurement techniques can provide single reading per measurement of either stress or strain or both, e.g. strain gauges and load cells. Digital photoelasticity can provide pointwise determination, and a visual image, of the intrinsic stress, which is a measure of the induced temporary state of birefringence. Lookup tables provide direct relation between the order of the photoelastic fringes and the stress anisotropy at each point of the test sample. Hence, the measurement of stress is achieved directly by comparing the captured pattern against the lookup tables.

The digital photoelastic technique is one of the common full-field stress visualisation and measurement methods of intrinsic stresses along polymeric fibres [4]. Photoelasticity evaluates the stress of models of obvious birefringent regions through polarisation optics. The loaded polymer might be investigated between crossed polarising filters. Within the transmitted light, structures of lines appear as a result of birefringence [5].

***Corresponding author: Taha Z. N. Sokkar**, Physics Department, Faculty of Science, Mansoura University, 35516 Mansoura, Egypt, E-mail: tzsokkar@mans.edu.eg
Ahmed A. Hamza, Mohammed A. El-Bakary and Amira A. S. Azzam, Physics Department, Faculty of Science, Mansoura University, 35516 Mansoura, Egypt

The formed photoelastic fringe pattern is due to alternately constructive interference between beams of light passing through a retarding phase region within the stretched polymeric material. Photoelastic fringe colour features are essential to interpret these patterns and convert their colour characteristics into stress values. While stress is implemented to a material, retardation among orthogonal polarisation states occurs due to the difference in velocity due to the change of index of refraction of fibres, known as stress birefringence [6]. As stress is induced in anisotropic materials, variations in the principle refractive index values are produced and therefore make the fibre anisotropic. Retardation between orthogonal polarisation states will occur for light incident on a stressed material.

Polymeric fibre drawing is an essential commercial technique. Drawn fibres are used in many industrial applications. The process of stretching enhances the overall properties of fibres making them more applicable and durable. The objective of drawing fibres is to orientate the molecular chains within the fibre, which increases their strength in the direction of stretching. The drawing techniques are essential to manufacture fibres with enhanced structures. It induces molecular orientation to a preferable direction and optical anisotropy [5, 7–10].

Interesting phenomena, e.g. necking and crazing, are observed peculiar to polymers during mechanical stretching. To better understand the formation of necking, distributions of molecular chains during the whole duration of drawing was previously studied [9]. The neck formation during cold drawing, resulting from severe local elongation of these molecular chains, impacts the microstructures and the mechanical properties of fibres [11, 12]. Also, the neck formation is related to material properties, which is associated with the micromechanisms of strain localisation [13].

The mechanical response of isotactic polypropylene (iPP) monofilaments is investigated using the digital photoelastic analysis of intrinsic stresses as a full-field visualisation technique. This technique provides a robust, rapid and highly accurate measurement of the intrinsic components of stress during the formation of the necking phenomenon. The main goals of this work are investigating the effect of different drawing speeds on stress patterns, which are the determined stress values for each photoelastic pattern, at a constant temperature of iPP fibres by using the photoelastic technique. And studying the stages of formation of necking during stretching using the photoelastic stress analysis, i.e. the stress measurements obtained using photoelastic patterns.

2 Materials and methods

In order to quantitatively characterise the phenomenon of fibre necking, samples of iPP fibres are mechanically processed at different stretching speeds. Figure 1a illustrates the optomechanical polariscope designed to collect photoelastic data of polymer fibres during different mechanical treatments. A monofilament of the iPP fibre is fixed to the stretching motors, M1 and M2. These stepper motors can stretch a sample of iPP fibres at 200 step/rev which produces a length change per single step, $\Delta L = \pm 0.16$ mm/step. The mechanical stretching process is controlled by a software designed to control different stretching parameters including stretching rate, mode and direction. The tested fibres are immersed in a liquid of refractive index $n_L = 1.500$ at 20 °C.

Software used is designed to control the optomechanical system. Figure 1b shows the flowchart of designed software. Software checks for valid communication signal between software and the optomechanical system. Experiment parameters, e.g. stretching speed and experiment procedures, are passed to the microcontroller of the

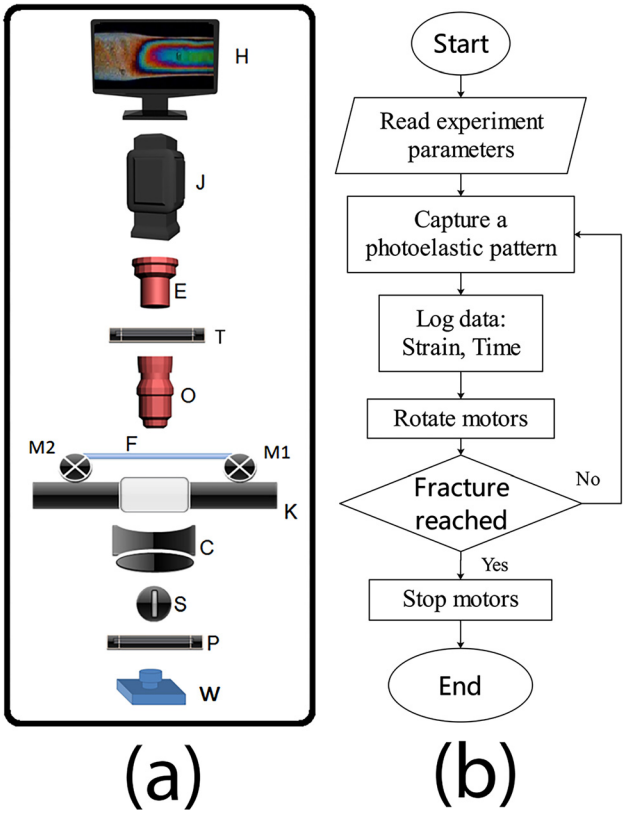

Figure 1: (a) The optomechanical polariscope designed to collect photoelastic data of polymer fibres during mechanical processing. (b) The flowchart of software designed to control the optomechanical polariscope. W, white light source; P, polariser; S, slit diaphragm; C, condenser lens; K, microscope stage; M1 and M2, stretching motors; F, fibre sample; O, objective lens; T, analyser; E, eyepiece; J, digital camera and H, PC screen showing a sample pattern.

system. Based on these parameters, the fibre is stretched until it fractures. In this study, the fibre is stretched at the room temperature. A temperature controller can be used to prevent fluctuations of temperature during the experiment, at accuracy = ±1 °C. The fibre is stretched by one step, then a photoelastic pattern is recorded, and the values of strain and speed are also recorded, simultaneously. Then, if the fibre had not reached its breaking point, the stretching continues. If the fracture point is reached, then the stretching process is stopped, and the photoelastic patterns are analysed for extracting the photoelastic order which is a good indicator of birefringence and principle stress difference.

3 Results and discussion

In digital photoelasticity, the measurable photoelastic order, N, is the main parameter for calculating the full-field distribution of the anisotropic intrinsic stress difference, ΔS, according to the following equation [14]:

$$\Delta S = (S_1 - S_2) = \frac{N}{2t}\frac{\lambda_0}{k}\frac{E}{1+\nu} \tag{1}$$

and the birefringence is given by the following equation:

$$\Delta n = C\ \Delta S \tag{2}$$

where S_1 and S_2 are the orthogonal principle components of stress. The following coefficients were previously measured for iPP fibres: E, the modulus of elasticity = 2 GPa; ν, Poisson's ratio = 0.21; k, strain-optic coefficient = 0.0082, refer to the studies by Galanti and Mantell [15] and Hamza et al [16]; t, the fibre thickness; C, the stress-optic coefficient = 1.23×10^{-9} Pa^{-1}, refer to the studies by Okada et al [17] and Inoue et al [18]; Δn, the optical birefringence and λ_0, the reference wavelength (λ_0 = 590 nm), which was proposed by Ajovalasit et al. [19] in the case of using the colour photoelastic analysis technique [4].

3.1 Comparison between birefringence measurements using two-beam interferometry and digital photoelasticity

In this work, we measured the photoelastic order which is a good indicator of birefringence values at different points inside the fibre. The two-beam Pluta polarising interference microscope is one of the major techniques for measuring the variations of birefringence inside thermally and mechanically treated fibres [20]. On the other hand, RGB photoelastic measurements of birefringence have the advantage over two-beam interferometry in many aspects. In order to clarify this point, the Pluta polarising interference microscope in its uniform-field mode is adjusted to produce photoelastic patterns of the test sample by replacing the Wollaston prisms with a microscope objective lens. After capturing the photoelastic patterns, with the sample in its place, the Pluta polarising interference microscope is switched back to its nonduplicating two-beam interference mode using the Wollaston prisms. Hence, a two-beam interference pattern is produced at the same region captured previously in the photoelastic mode.

Figures 2a, b depicts the captured patterns for the case of two-beam interference and a photoelastic pattern showing the same necking region in order to compare the calculated phase map at this region. Photoelastic lookup tables are used to map the pixel colour values to the photoelastic order, N, at any point, see Figure 2c. It consists of pairs; each pair consists of a colour (RGB value) and a photoelastic order, N, value. Each colour pixel is compared against the lookup table pairs to find the nearest colour match by finding the minimum colour distance (error function) [19]:

$$e = \sqrt{(R - R_t)^2 + (G - G_t)^2 + (B - B_t)^2} \tag{3}$$

where the subscript (t) denotes a lookup table value. The colour of the pixel is replaced with the corresponding photoelastic order value, N. The final result is a map of the photoelastic orders based on the colours of the photoelastic pattern. Accordingly, the captured photoelastic pattern is compared pointwise to a preevaluated colour-order pairs known as a lookup table. Each (RGB) value of a pixel will be replaced by a value (N) denoting the order value at this pixel based on its colour value.

In Figure 3, we illustrate the main advantage of digital photoelasticity which is the pointwise calculation of birefringence values. On the other hand, online two-beam interferometry usually uses Fourier transform for obtaining the phase distribution across the fibre. Usually, Fourier transform produces acceptable phase maps for low-gradient phase values, e.g. uniform fibre samples. But for the case of increased phase gradients, as in necking regions, the measured phase values show deviations from the true phase values due to the nature of filtering in the frequency domain.

A careful inspection of the birefringence values produced by the digital RGB photoelasticity showed a smooth transition of the phase values at the neck region (which are considered as high phase gradient regions). Accordingly, the digital RGB photoelastic determination of the birefringence values is more reliable than two-beam interferometric techniques for online characterisation of birefringence profile of fibres, in addition to being a more

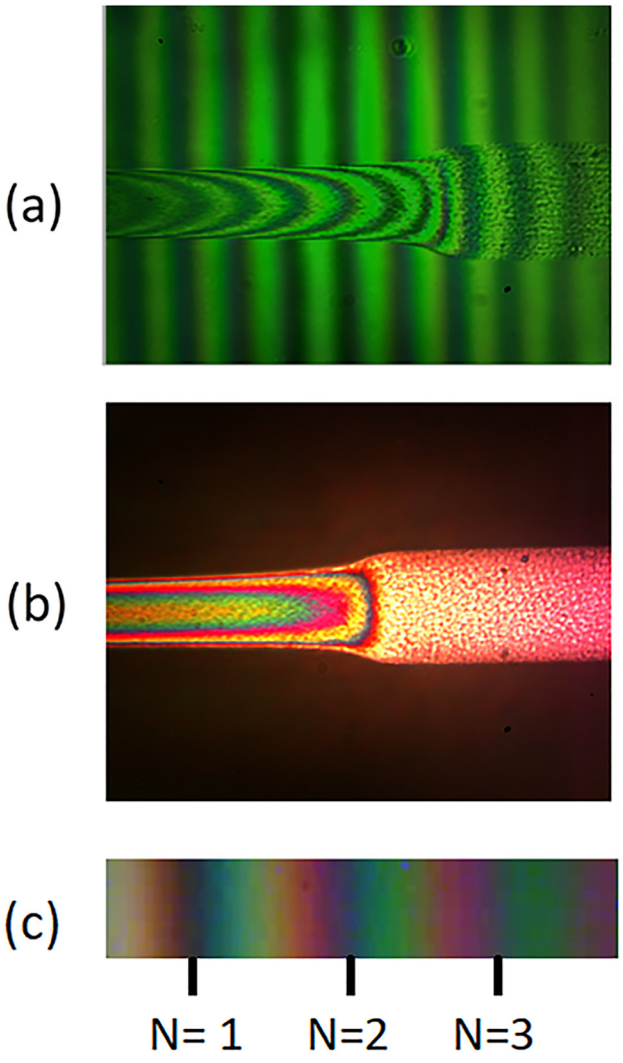

Figure 2: The captured patterns for the case of (a) two-beam interference and (b) a photoelastic pattern of the same necking region. (c) The lookup table used to calculate the photoelastic order, *N*, represented as a relation between the photoelastic order, *N*, represented by the *x*-axis and the RGB colour values of each pixel along the *x*-axis.

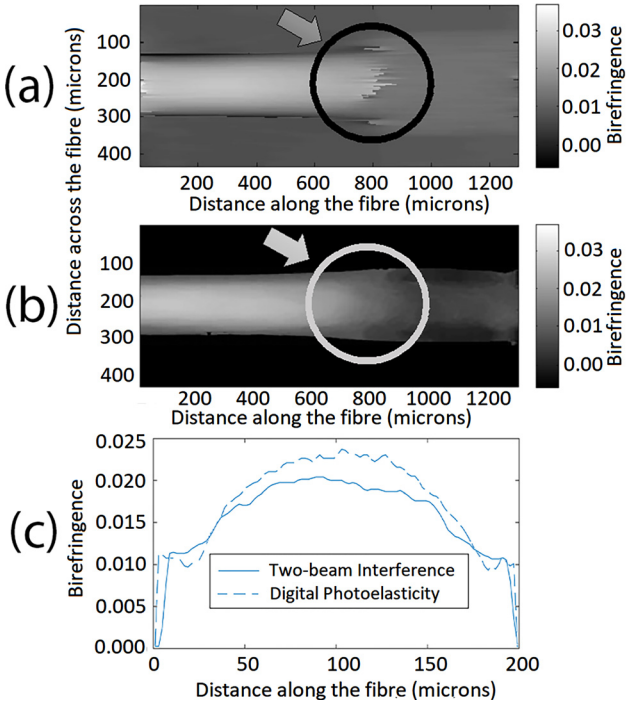

Figure 3: The birefringence values calculated using (a) Fourier analysis of two-beam interferogram, (b) photoelastic analysis, (c) the birefringence profile calculated from the two-beam interference pattern (solid line measured at a cross-sectional line at a distance = 680 μm measured from the left of the field of view, and the birefringence profile calculated from the photoelastic pattern [dashed line]) measured at the same cross-sectional line.

direct and rapid technique. Also, the fibre geometry can be determined using digital photoelastic patterns better than two-beam interference patterns since digital photoelasticity does not depend on the presence of carrier fringes, while two-beam interference patterns contains reference fringes in addition to the deformed regions which makes fibre-boundary recognition process more difficult. Thus, digital photoelasticity is recommended for online characterisation of a necking deformation. On the other hand, for smooth regions along the fibre, e.g. before and after the neck region, there is a negligible deviation between the birefringence profile obtained using digital photoelasticity and the birefringence values obtained using digital interferometry, as depicted in Figure 3c. Accordingly, digital photoelasticity provides a reliable determination of the birefringence profiles of high accuracy nearly equal to the obtained profiles using the two-beam Pluta polarising interference microscope.

3.2 The effect of stretching speeds on necking initiation

A monofilament of the iPP fibre is fixed to the clamps of the stretching motors. The heater of the thermomechanical assembly is used to fix the ambient temperature to 19 °C. The motors are rotated to stretch the iPP fibre until a neck is formed. The stretching continues until the neck propagates and is no longer visible in the observed field of the microscope. The process is repeated for identical monofilaments at different stretching speeds: v = 0.16, 0.79, 1.1, 1.42, 1.73, 2.05 (mm/s). Figure 4 depicts the photoelastic patterns of iPP fibres mechanically stretched at different speeds. For each speed, photoelastic patterns are captured for three

different fibre states. The initial undrawn fibre state, a pattern showing a necking deformation nearly in the middle of the field view and a pattern for the region just after the necking region leaves the field of view.

In order to enhance the accuracy of calculations, each photoelastic pattern is processed for reducing noise and enhancing colour features along the fibre using suitable image processing techniques [4]. Then, the captured photoelastic patterns are analysed using lookup tables to find the photoelastic order, N, which is the main parameter for calculating the intrinsic stress anisotropy, ΔS. Figure 5 shows the calculated photoelastic order, N, for iPP samples stretched at different speeds. The black pixels are points having photoelastic orders, $N = 0$, while the white pixels

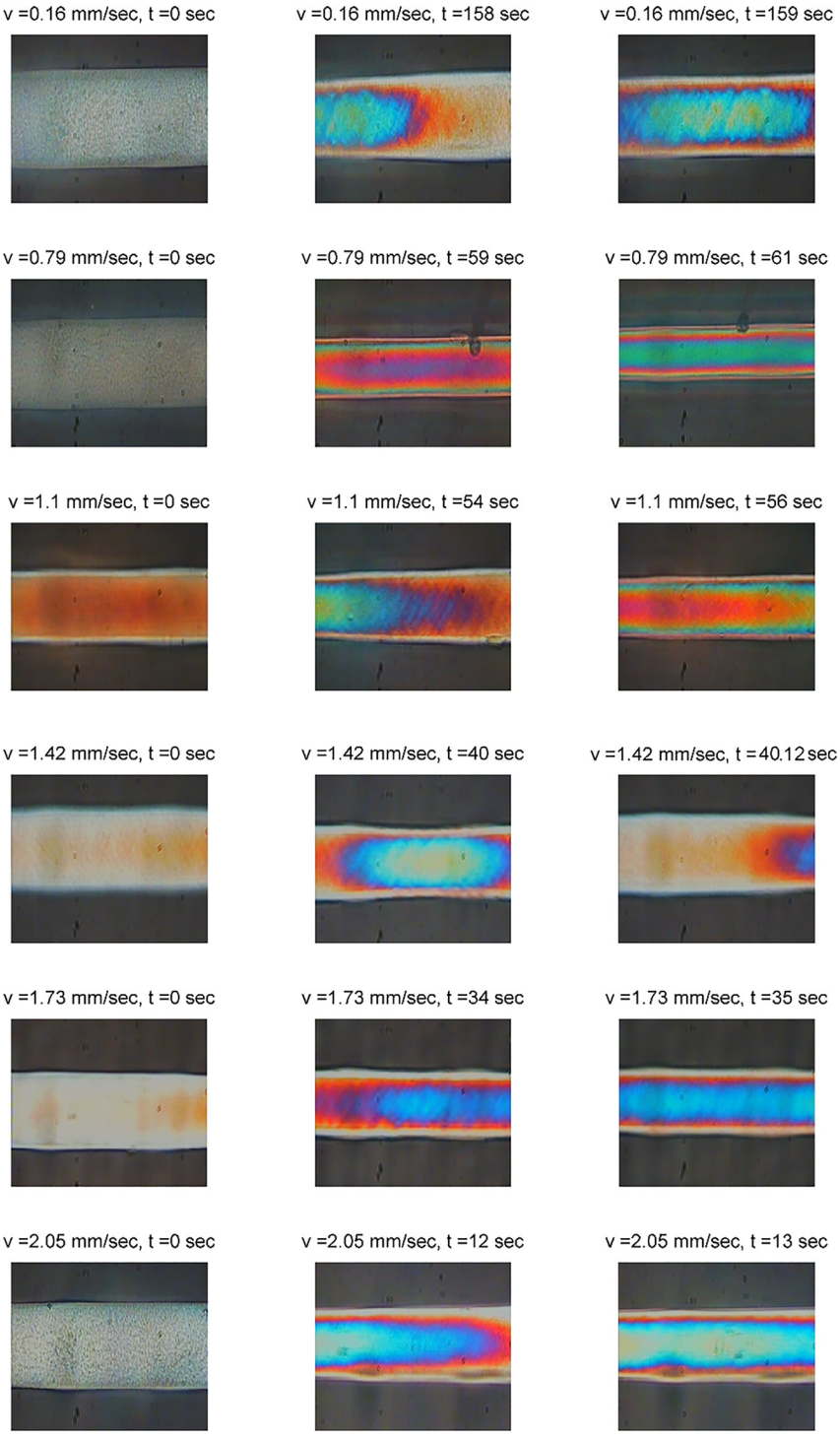

Figure 4: The photoelastic patterns of isotactic polypropylene (iPP) fibres mechanically stretched at different speeds: $v = 0.16$ mm/s; $v = 0.79$ mm/s; $v = 1.1$ mm/s; $v = 1.42$ mm/s; $v = 1.73$ mm/s and $v = 2.05$ mm/s.

denote photoelastic orders, $N = 3$: the intermediate grey pixels refer to orders between 0 and 3. Accordingly, it is clear that undrawn patterns showed relatively small photoelastic orders ($N < 1$) indicating low intrinsic stress anisotropy, ΔS.

Upon further stretching, the intrinsic stress anisotropy, ΔS, increases and becomes localised at the neck, reaching photoelastic orders between 1.5 and 2.5. The photoelastic patterns captured after the necking regions showed higher photoelastic orders ($N \approx 3$) with radial symmetry across the fibre indicating that the intrinsic stresses which are higher at the central layers gradually decrease toward the outer layers. Also, a noticeable decrease of the intrinsic stress anisotropy is observed by increasing the stretching speeds for photoelastic patterns containing necking and after the passage of the necking. This implies that the increased speed of stretching results in lower localised intrinsic stresses during the formation of necking. Although after the observed necking region there is an increasing trend of the intrinsic stresses, the overall intrinsic stresses have lower values for higher speeds of stretching.

In Figure 6, a gradual increase of the fibre stress anisotropy is detected, which extends from the undrawn part of the fibre to the neck region. The highest value of the intrinsic stress anisotropy is localised at the centre of the neck. Figure 7a shows the calculated birefringence values from the measured intrinsic stress anisotropy at the middle of the necking region at different stretching speeds. This

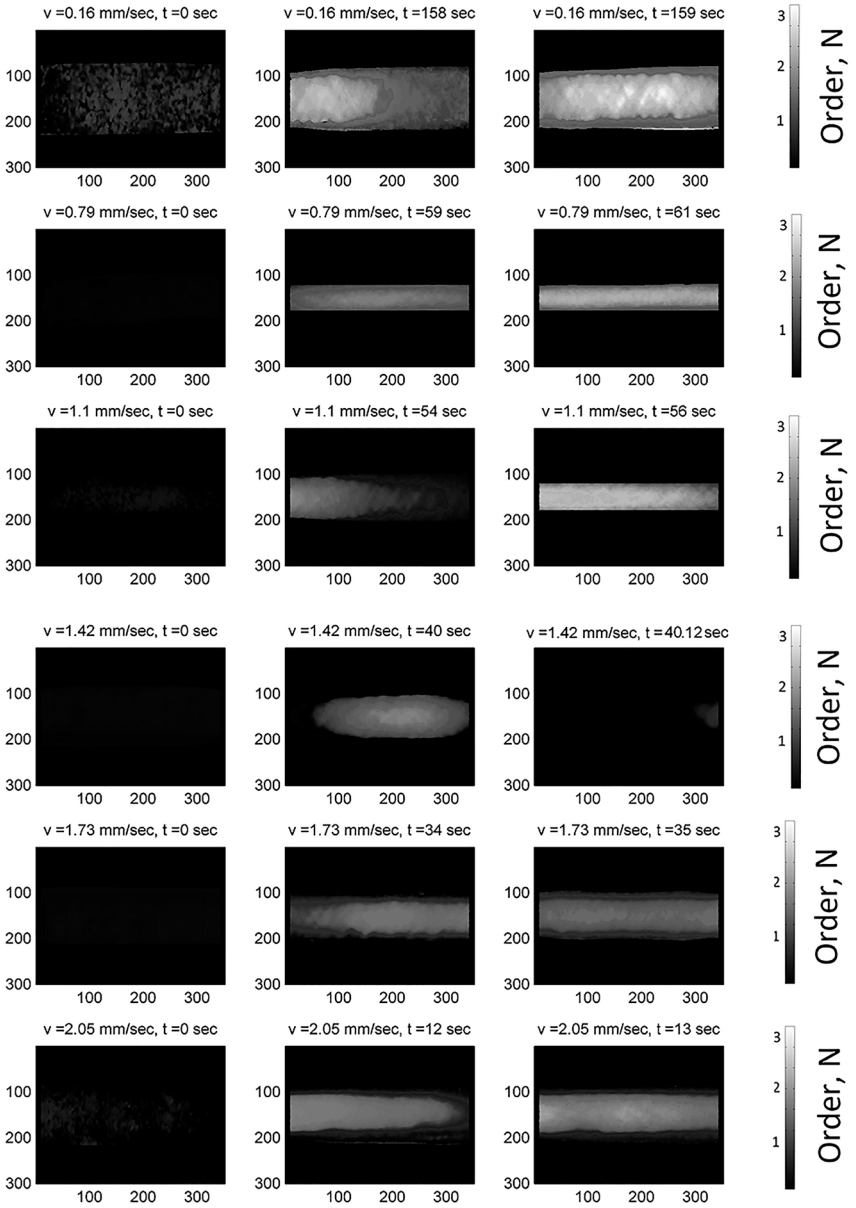

Figure 5: The photoelastic order of iPP fibres mechanically stretched at different speeds: $v = 0.16$ mm/s; $v = 0.79$ mm/s; $v = 1.1$ mm/s; $v = 1.42$ mm/s; $v = 1.73$ mm/s and $v = 2.05$ mm/s. The x-axis represents the distance along the fibre in microns, and the y-axis represents the distance across the fibre axis in microns. iPP, isotactic polypropylene.

figure clearly shows that, the necking is initiated at relatively high intrinsic stress anisotropy, ΔS, for lower stretching speeds, which decreases by increasing the stretching speed. Another advantage of photoelastic patterns is the direct detection of necking initiation times. Figure 7b shows the necking initiation times as a function of the stretching speed. It is noticed that increasing the stretching speed decreases the time required to initiate a neck region inside the fibre. Accordingly, increasing the stretching speeds causes faster alignment of the molecular chains inside the fibre, and the result is that less time required to initiate the necking region.

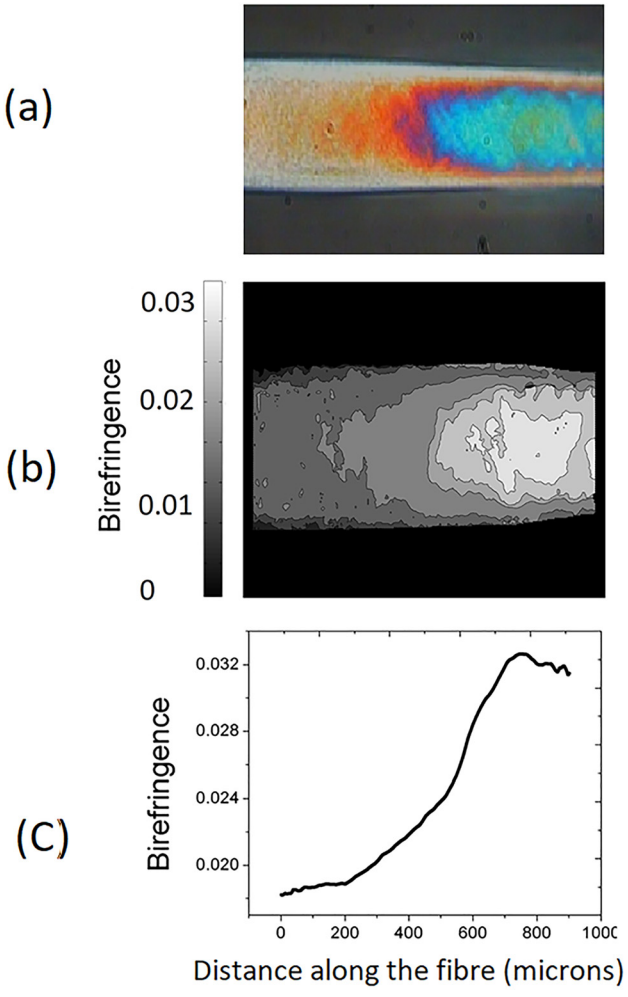

Figure 6: The intrinsic stress anisotropy in terms of birefringence of a typical necking observed at low stretching speed ($v = 0.157$ mm/s). (a) The photoelastic pattern of the formed necking phenomenon; (b) a 2D map of the distribution of the birefringence values along the fibre axis; (c) the birefringence values at the central layer of the fibre along its axis during the formation of the necking phenomenon.

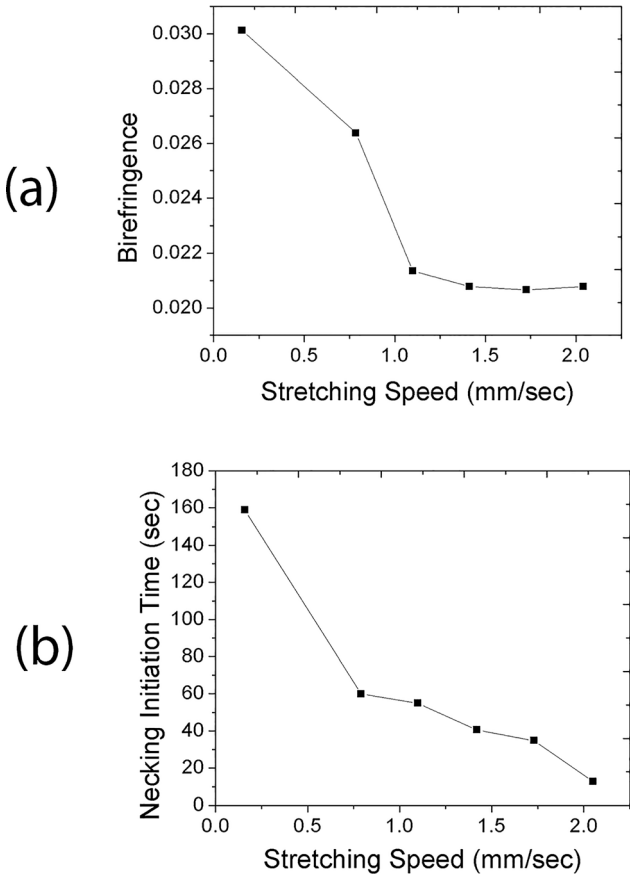

Figure 7: (a) The calculated birefringence values from the measured intrinsic stress anisotropy at the middle of the necking region at different stretching speeds: $v = 0.16$ mm/s; $v = 0.79$ mm/s; $v = 1.1$ mm/s; $v = 1.42$ mm/s; $v = 1.73$ mm/s and $v = 2.05$ mm/s. (b) The necking initiation times as a function of the stretching speeds: $v = 0.16$ mm/s; $v = 0.79$ mm/s; $v = 1.1$ mm/s; $v = 1.42$ mm/s; $v = 1.73$ mm/s and $v = 2.05$ mm/s.

3.3 Early stages of necking growth

Necking is a strong precursor of material failure. Understanding the necking behaviour of fibres is essential to control the conditions leading to material failure. In this work, we were able to observe the birth of necking photoelastically. This observation provides information on the state of stress at regions where necking is expected to initiate. Consequently, we were able to predict the initiation of necking based on intrinsic stress measurements.

Careful stretching of the iPP fibres allowed us to detect the birth and growth of necking. The fibre samples are fixed to the stretching motors, and the fibre is moved so that its centre point is observed at the objective lens field of view. Slow stretching (speed = 0.16 mm/s) of the fibre at this point facilitates detection of the early stages of necking growth. Figure 8 shows the captured photoelastic patterns

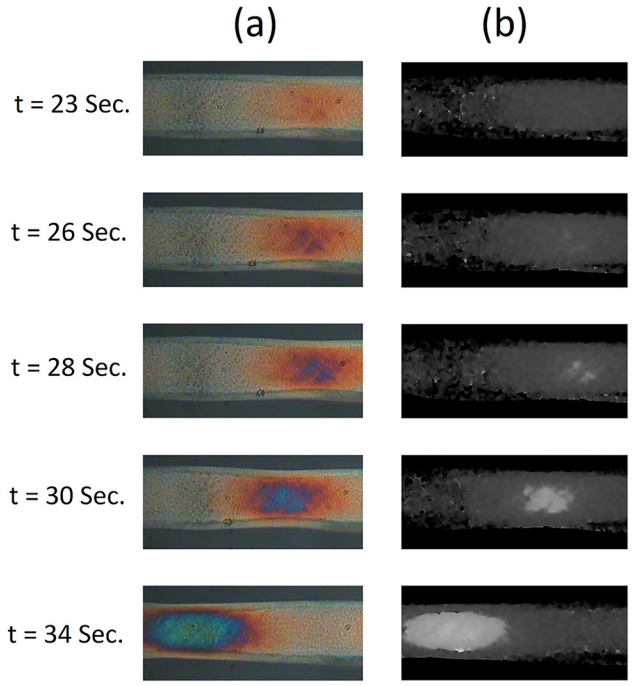

Figure 8: (a) The captured photoelastic patterns and (b) the calculated photoelastic orders of the fibre at early stages of necking formation.

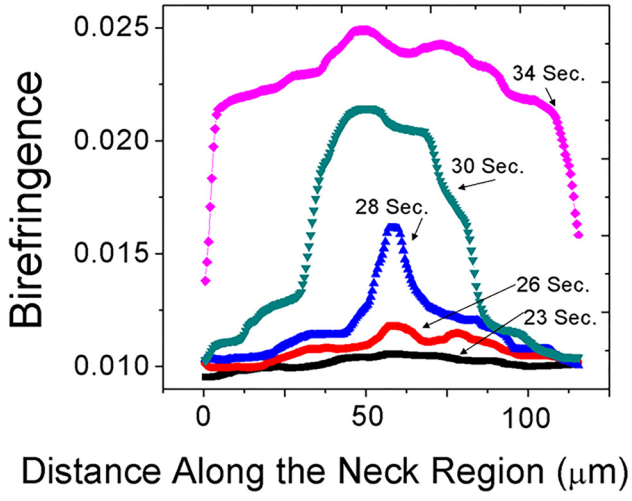

Figure 9: The birefringence values of the fibre at the early stages of necking formation.

of the fibre at the early stages of necking formation. These photoelastic patterns are enhanced and analysed to find the photoelastic order at the region of the growing necking. This figure also depicts the calculated photoelastic orders of the fibre during the formation of the necking region, which is a measure of the intrinsic stress anisotropy, ΔS. The necking phenomenon initiates as a localised rise of the intrinsic stress at a certain region. Continuous stretching concentrates the intrinsic stress at a small area of the selected region. The concentrated localised stresses are propagated to the adjacent areas, and the intrinsic stress increases rapidly at the selected region compared to other parts of the stretched fibre. Finally, the region of high localised intrinsic stress anisotropy expands to form a neck-shoulder morphology, and a necking is visually observed. These stages are described in terms of the calculated birefringence values at different stages of necking initiation which is depicted in Figure 9.

3.4 Formation of multiple necking regions

In our study, the necking phenomenon may be initiated at different regions synchronously during stretching. In other words, in some cases, the localised increase in the intrinsic stress anisotropy responsible for the formation of necking may occur at different positions rather than at one region [21]. We are able to detect the formation of multiple necking

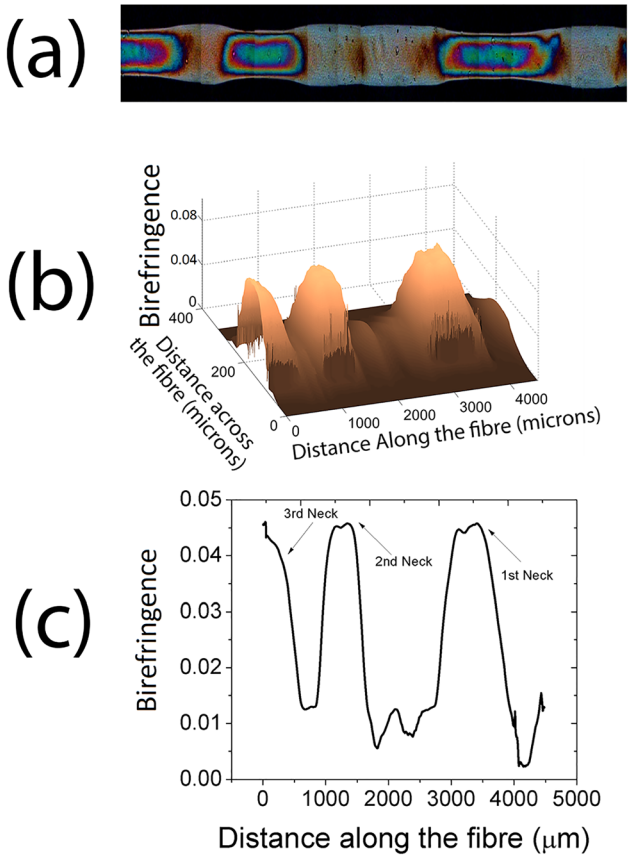

Figure 10: (a) The photoelastic pattern of the multiple-necking phenomenon constructed by digitally stitching several photoelastic patterns captured along the multiple necking region. (b) The 3D birefringence profile of the multiple necking region and (c) the values of the birefringence for the central layers along the fibre.

by stretching an iPP fibre sample at a stretching speed of 0.471 mm/s and at temperature T = 25 °C. The stretched sample is investigated using a polariscope to capture the photoelastic patterns of the fibre during stretching.

The continuous capturing of the photoelastic patterns during stretching allowed us to reconstruct the necking regions along the fibre during stretching. Figure 10a shows the reconstructed photoelastic pattern of the multiple necking phenomenon. Our designed software is able to stitch, enhance and analyse the captured photoelastic frames. The photoelastic order, N, is calculated along the fibre during the formation of multiple necking, then the birefringence is calculated at different points along the multiple necking region, which is given in Figures 10b, c. According to this figure, although these synchronous necking regions were observed at different positions, they nearly initiated at the same birefringence values, Δn, approximately at the value of the photoelastic order, $N \approx 4$. The same photoelastic order is observed for all the necking regions observed in a multiple necking deformation, which implies that the same stress state should be met in order to form a necking. This condition is also suggested in case of single necking formation which confirms that the current stress state can be used as a reliable indication of necking formation.

4 Conclusions

A quantitative photoelastic study of the necking formation in iPP fibres is introduced in this study. The effect of increasing the stretching speed on necking is investigated quantitatively. Higher speeds of stretching result in the initiation of necking at smaller intrinsic stress anisotropy. Also, fast stretching causes faster arrangement of molecular chains and hence decreases the time required for necking initiation.

Using the distinctive colour patterns of photoelasticity, the early stages of necking formation can be visually detected. This advantage provided a thorough understanding of how localised intrinsic stress anisotropy grows to form a necking region. We were able to detect the formation of multiple necking using the digital photoelastic stress analysis. These multiple necking regions were nearly initiated at the same intrinsic stress anisotropy, which suggests that these multiple necks are initiated using the same formation mechanism and conditions applied if there is only a single necking region.

The provided information on the behaviour of the necking phenomenon during different thermal and mechanical processing methods provides valuable knowledge of detection and avoidance of the necking phenomenon, especially for industrial applications in which enhanced fibre properties are accomplished via mechanical stretching and thermal treatments.

In this work, we characterised the failure by necking behaviour of the iPP fibres since it is widely used in many commercial and industrial applications. In the future work, we are considering applying the used photoelastic technique for characterising the failure behaviour of other common polymeric and textile fibres, e.g. polyethylene terephthalate and poly(methyl methacrylate).

Acknowledgments: The authors would like to express their gratitude to the late Prof. K. A. El-Farahaty for the useful discussions and her help during the work and preparation of this article.
Author contribution: All the authors have accepted responsibility for the entire content of this submitted manuscript and approved submission.
Research funding: None declared.
Conflict of interest statement: The authors declare no conflicts of interest regarding this article.

References

1. Williams J. *Stress Analysis of Polymers (Book-Stress Analysis of Polymers*; Halsted Press: New York, 1973; pp 283.
2. Soloman S. *Sensors Handbook*; McGraw-Hill, Inc.: New York, United States, 2009.
3. Orr J. F., Shelton J. C. *Optical Measurement Methods in Biomechanics*; Springer: London, United Kingdom, 1997.
4. Ramesh K. *Digital Photoelasticity: Advanced Techniques and Applications*; Springer-Verlag: Berlin, 2000.
5. Sperling L. H. *Introduction to Physical Polymer Science*; John Wiley & Sons: New Jersey, United States, 2005.
6. Milby E. *Investigating Stress Birefringence Using Photoelasticity*; The University of Arizona: Tempe, AZ, USA, 2011.
7. Hamza A., Sokkar T., El-Bakary M. Detection of the variation of the optical and geometrical parameters of fibres due to the cold drawing process. *Meas. Sci. Technol.* 2004, *15*, 831.
8. Sokkar T., El-Bakary M., Ali A. The influence of mechanical cold drawing and drawing velocity on the molecular structure of isotactic polypropylene fiber. *J. Appl. Polym. Sci.* 2013, *127*, 1105–1113.
9. Sokkar T., El-Din M. S., El-Tawargy A. On young's modulus profile across anisotropic nonhomogeneous polymeric fibre using automatic transverse interferometric method. *Opt. Laser. Eng.* 2012, *50*, 1223–1229.
10. Sokkar T., El-Farahaty K., Azzam A. On-line interferometric study on the mechanical fracture behaviour by crazing observed in stretched polypropylene fibres. *Fibers Polym.* 2014, *15*, 605–613.
11. Andrzej Z. *Fundamentals of Fiber Formation*; Wiley and Sons Pub.: New York, 1976.

12. Chung K., Yoon H., Youn J. R. Neck formation in drawing processes of fibers. *Fibers Polym.* 2001, *2*, 18–21.
13. Turi E. *Thermal Characterization of Polymeric Materials*; Elsevier: New York, United States, 2012.
14. Burger C. Photoelasticity. In *Handbook on Experimental Mechanics*; Kobayashi A. S., Ed. Prentice-Hall: New Jersey, United States, 1993; pp. 165–266.
15. Galanti A. V., Mantell C. L. *Polypropylene Fibers and Films*; Springer: New York, 1965.
16. Hamza A., Fouda I., Sokkar T., Shahin M., Seisa E. Optothermal properties of fibres. *J. Mater. Sci.* 1995, *30*, 2597–2604.
17. Okada Y., Urakawa O., Inoue T. Reliability of intrinsic birefringence estimated via the modified stress-optical rule. *Polym. J.* 2016, *48*, 1073.
18. Inoue T., Mizukami Y., Okamoto H., Matsui H., Watanabe H., Kanaya T., Osaki K. Dynamic birefringence of vinyl polymers. *Macromolecules* 1996, *29*, 6240–6245.
19. Ajovalasit A., Barone S., Petrucci G. Towards RGB photoelasticity: full-field automated photoelasticity in white light. *Exp. Mech.* 1995, *35*, 193–200.
20. Pluta M. A double refracting interference microscope with continuously variable amount and direction of wavefront shear. *Opt. Acta Int. J. Opt.* 1971, *18*, 661–675.
21. Sokkar T., El-Tonsy M., El-Bakary M., El-Morsy M., Ali A. A novel video opto-mechanical (VOM) device for studying the effect of stretching speed on the optical and structural properties of fibers. *Opt. Laser. Technol.* 2009, *41*, 310–317.